THE JOURNAL OF PHYSICAL CHEMISTRY C

Article

Cite This: J. Phys. Chem. C 2019, 123, 5776−5781

pubs.acs.org/JPCC

Organic Molecular Tuning of Many-Body Interaction Energies in Air-Suspended Carbon Nanotubes

Shunsuke Tanaka,[†,‡] Keigo Otsuka,[†,‡] Kensuke Kimura,[§,∥] Akihiro Ishii,[†,‡] Hiroshi Imada,[§] Yousoo Kim,[§] and Yuichiro K. Kato*[,†,‡]

[†]Quantum Optoelectronics Research Team, RIKEN Center for Advanced Photonics, Saitama 351-0198, Japan

[‡]Nanoscale Quantum Photonics Laboratory and [§]Surface and Interface Science Laboratory, RIKEN Cluster for Pioneering Research, Saitama 351-0198, Japan

[∥]Department of Advanced Materials Science, School of Frontier Sciences, The University of Tokyo, Chiba 277-8561, Japan

ABSTRACT: We investigate adsorption effects of copper phthalocyanine molecules on excitons and trions in air-suspended carbon nanotubes. Using photoluminescence excitation spectroscopy, we observe that exciton energy red-shifts gradually with the molecular deposition thickness. The trion emission is also observed at large deposition amounts, which indicates charge transfer between the phthalocyanine molecules and carbon nanotubes. Analysis of the spectra for individual tubes reveals a correlation between the exciton−trion energy separation and the exciton emission energy, showing that the many-body interaction energies scale similarly with the molecular dielectric screening.

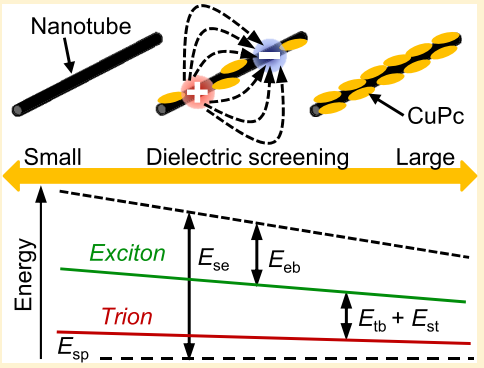

INTRODUCTION

Single-walled carbon nanotubes (CNTs) have attracted considerable attention due to their remarkable physical and electronic properties, and much effort has been devoted to functionalize CNTs for expanding their capabilities.[1−4] In particular, noncovalent functionalization with organic molecules is a powerful strategy for developing CNT-based devices such as photovoltaics and photodetectors.[5−10] The interactions between the organic molecules and CNTs are considered to be less perturbative compared to covalent modification, and therefore the outstanding properties of CNTs can be preserved. Organic molecules such as porphyrin and phthalocyanine couple to nanotubes through $\pi-\pi$ interactions to modify the charge density of CNTs, while the emission energy is reduced due to the molecular screening.[11−16] Furthermore, there are unique exciton dynamics at the organic molecule/CNT interface including energy and charge transfer.[14,17−22]

In the measurements performed for nanotubes in solutions, however, the existence of solvent molecules inevitably complicate the interpretation by influencing the interactions. Additionally, the solvents themselves provide molecular screening, reducing the dielectric effects of the organic molecules. Investigation of molecular adsorption on air-suspended nanotubes would provide invaluable information toward fundamental understanding of the adsorption effects, as thermal evaporation techniques[23,24] allow for molecular deposition without introducing other molecules. The use of pristine tubes should further enable drastic dielectric modification for developing noncovalently functionalized CNT devices.

Here, we demonstrate control over many-body interaction energies in air-suspended CNTs by copper phthalocyanine (CuPc) molecule adsorption. The molecules are deposited on chirality-assigned CNTs by thermal evaporation, and we perform photoluminescence (PL) spectroscopy of the CuPc/CNT hybrid. From the averaged PL and PL excitation (PLE) spectra for various chiralities, we find that the E_{11} and E_{22} resonances red-shift with increasing deposition thickness. Furthermore, a new emission peak is observed at an energy below the E_{11} peak, which is attributed to trion emission. Data from individual tubes reveal a good correlation between exciton−trion energy separation and the E_{11} energy, suggesting the existence of a universal relationship. We consider a model assuming power law scaling of the interaction energies with dielectric constant to explain the observed correlation.

EXPERIMENTAL SECTION

Air-Suspended CNTs. Our suspended CNTs are grown over trenches on bare Si substrates (Figure 1a). We perform electron beam lithography and dry etching to form the trenches, and another electron beam lithography step defines catalyst areas near the trenches. Fe(III) acetylacetonate and fumed silica dispersed in ethanol are spin-coated as catalyst for

Received: December 28, 2018
Revised: February 12, 2019
Published: February 13, 2019

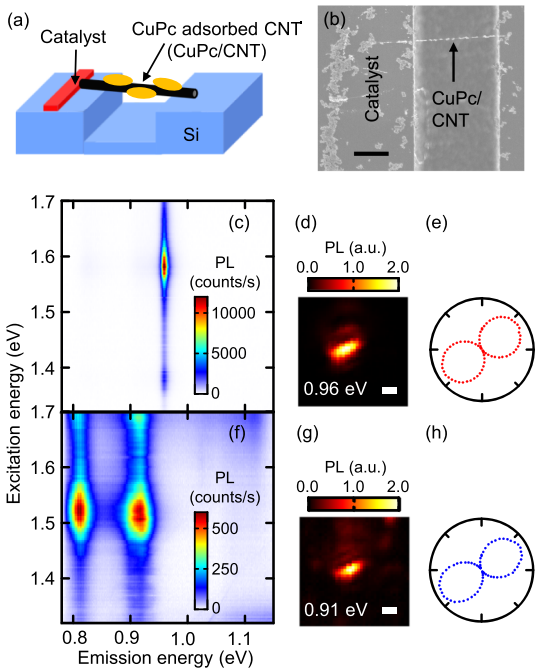

Figure 1. (a) Schematic image of our sample. (b) Scanning electron microscope image of a CuPc/CNT hybrid. (c–e) PLE map, PL image, and laser polarization angle dependence, respectively, for a (9,7) nanotube in the 26 nm sample before CuPc deposition. For (d,e), the PL intensity is obtained by integrating PL over a 10 meV wide spectral window centered at 0.96 eV. (f–h) PLE map, PL image, and laser polarization angle dependence, respectively, for the same tube after the deposition. For (g,h), the PL intensity is obtained by integrating PL over a 10 meV wide spectral window centered at 0.91 eV. (b,d,g) Scale bars are 1 μm. Panels (c–e) are taken with P = 5 μW, and (f–h) are taken with P = 300 μW.

CNT growth. CNTs are synthesized by alcohol chemical vapor deposition at 800 °C for 1 min.[25]

PL Microscopy. The PL measurements are carried out with a home-built confocal microspectroscopy system.[25,26] A continuous-wave Ti:sapphire laser is used for excitation with a power P, and an objective lens with a numerical aperture of 0.8 and a working distance of 3.4 mm focuses the laser onto the sample. The linear polarization of the excitation laser is rotated using a half-wave plate and PL from the sample is detected by an InGaAs photodiode array detector attached to a spectrometer. The laser polarization is parallel to the tube axis for measuring PLE maps and PL images. All measurements are conducted at room temperature in dry nitrogen.

Sample Characterization before CuPc Deposition. We characterize the suspended nanotubes before the deposition. CNTs are located by line scans along the trenches, and PLE measurements are performed. We check whether only a single peak is observed in the emission spectrum and whether the E_{11} and E_{22} resonance energies match tabulated data for air-suspended nanotubes.[25] If a nanotube satisfies these conditions, the position and the chirality of the nanotube are recorded into a list for the measurements after the deposition.

CuPc Deposition on Nanotubes. After the characterization, the sample is placed in a vacuum chamber for evaporation of CuPc (Sigma-Aldrich) and is kept at about 80 °C for 10 min to remove air molecules before the evaporation. CuPc molecules are deposited on suspended CNTs in the chamber at room temperature using an evaporator heated to 480–520 °C under a vacuum of less than 10^{-4} Pa. A glass slide is also placed in the chamber to quantify the deposition thickness from absorbance of CuPc peak at 2.0 eV.[27] Calibration is performed by measuring the actual thickness by a surface profiler for two CuPc films with 80 and 167 nm. Four samples with different deposition amounts are prepared by changing the evaporation time, with nominal thickness on the substrate of 3, 7, 16, and 26 nm.

RESULTS AND DISCUSSION

CuPc Adsorption Effects. In order to investigate the molecular adsorption effects, we compare the nanotubes before and after molecular deposition. A scanning electron microscopy image of a typical CNT after the evaporation is shown in Figure 1b. Bright spots are observed sparsely on the suspended CNTs, indicating inhomogeneous adsorption of CuPc. Figure 1c–h shows PL spectra, PL images, and polarization dependence for a suspended CNT before and after CuPc deposition for the 26 nm sample. We note that the data before deposition have been taken prior to heating and therefore air molecules are adsorbed. In the PLE map before the deposition (Figure 1c), the emission occurs at the E_{11} energy and the E_{22} transition can be observed as a resonance in the excitation energy. The values for the E_{11} and E_{22} resonances are consistent with those for a (9,7) air-suspended nanotube,[25] indicating that air-molecules such as water are adsorbed.[28,29] Figure 1f shows a PLE map of the same tube after the deposition, and we find differences in the peak energy, the line width, and the intensity. Both of the E_{11} and E_{22} resonances show red-shift as well as broadening, and the PL intensity decreases significantly with the molecular adsorption. Additionally, a new emission band appears in an energy region below the E_{11} emission. The PL image of the molecular adsorbed nanotube is slightly smaller compared to that before the evaporation (Figure 1g,d), which is likely due to the inhomogeneous adsorption as observed in Figure 1b. In comparison, the laser polarization dependence does not change before and after the deposition (Figure 1e,h).

***E_{11}* and *E_{22}* Resonance Energy Shifts.** The PLE maps of the nanotubes for the four samples are measured to examine the deposition amount dependence of the adsorption effects. We integrate the PLE maps for each nanotube along the excitation and emission energy axes to obtain PL and PLE spectra, respectively, and the spectra for nanotubes with the same chiralities are averaged within each sample. The ensemble averaged PL and PLE spectra for (9,7) tubes are shown in Figure 2a,b, respectively. In the PL spectra (Figure 2a), the intensity decreases and the E_{11} resonance energy red-shifts with the increase of the deposition thickness. Two peaks are observed for the 3 nm sample, corresponding to emission from regions of nanotubes with and without the CuPc molecule adsorption. In contrast, the E_{11} emission shows only one peak in the PL spectrum for the 7 nm sample, suggesting that the nanotube surface is fully covered with the molecules. For samples thicker than 7 nm, the new emission band is observed as in Figure 1f, and we will refer to this peak as the T emission. While the relative intensity of the T emission becomes higher compared to the E_{11} emission as the deposition amount increases, the absolute intensity does not seem to depend much on the amount of CuPc molecules.

In the PLE spectra (Figure 2b), the E_{22} resonance also red-shifts with increasing deposition thickness, and the simultaneous red shifts for the E_{11} and E_{22} resonances can be

DOI: 10.1021/acs.jpcc.8b12496
J. Phys. Chem. C 2019, 123, 5776–5781

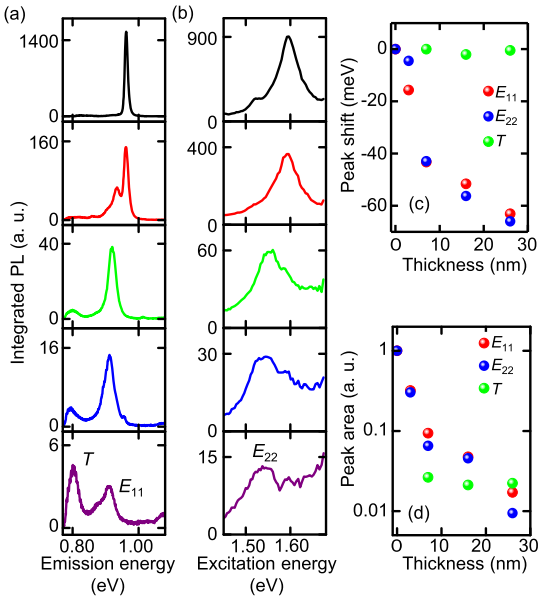

Figure 2. (a,b) Ensemble averaged PL and PLE spectra, respectively, for (9,7) tubes of the samples before deposition (black), 3 nm sample (red), 7 nm sample (green), 16 nm sample (blue), and 26 nm sample (purple). We measure 3−10 nanotubes for each sample and check that the same tube is measured before and after the deposition from the location and the laser polarization dependence. The nanotubes before and after the deposition are measured with P = 100 μW and P = 300 μW, respectively. The peak shift and peak area obtained from the fitting are shown in (c,d), respectively. The E_{11} and E_{22} peak shifts are compared to the peak energies before the deposition, and the E_{11} and E_{22} peak areas are normalized by those before the deposition. The peak shift for the T emission is compared to the peak energy for the 7 nm sample, and the peak area for the T emission is normalized by that for the E_{11} resonance before the deposition. The error bars are smaller than the symbols.

explained by the molecular dielectric screening.[29,30] For the 26 nm sample, the E_{22} resonance peak is on top of a broad background slope, which may be attributed to the tail of the CuPc absorption peak at 2.0 eV.[27] Exciton transfer from CuPc aggregates to CNTs would be consistent with the appearance of the absorption tail in the PLE spectra.[11,17] It has been suggested that the exciton transfer time is less than 100 fs in noncovalently bound nanotube/porphyrin hybrids,[14] and therefore the exciton transfer from the CuPc molecules to the nanotubes could occur before the intersystem crossing process (~500 fs).[31]

To evaluate the E_{11}, E_{22}, and T emission energy shifts for each sample, we extract the peak positions by fitting the ensemble averaged PL and PLE spectra. A Lorentz function is used to fit the E_{11} resonance in the PL spectra, except for the 3 nm sample where two Lorentz functions are used to obtain a weighted average of the E_{11} emission energy. The T emission band is also fitted by a Lorentz function for the PL spectra of the samples with more than 7 nm thickness. For the 3 nm sample, there is a difficulty for distinguishing the new emission band from K-momentum exciton emission band[32] due to the low intensity. In the case of the PLE spectra, we extract the E_{22} resonance energy by fitting with a Lorentzian on top of a linear function. In Figure 2c, we plot the energy shifts of the E_{11} and E_{22} resonances for (9,7) nanotubes relative to the energies before the evaporation. We note that the energy shifts are induced by changing the surface molecules from the air molecules to the CuPc molecules. The shifts show similar behavior, and the energies decrease monotonically with the deposition thickness. The E_{11} energy shifts by more than 60 meV, which is considerably larger than the shift caused by organic molecule adsorption in solutions (~20 meV).[11,14] The peak areas obtained from the fitting are also shown in Figure 2d, drastically decreasing as the thickness increases. A possible cause for the intensity reduction is carrier-induced PL quenching[28,33,34] as charge transfer between a metal-phthalocyanine and a CNT has been predicted by a density functional calculation.[12] The energy shift and peak area for the T emission are also plotted in Figure 2c,d, respectively, and both the energy and intensity roughly stay constant.

Using the same analysis procedure, the E_{11} and E_{22} resonance energies for various chiralities are obtained (Figure 3a). Red shifts of both resonances are observed for all

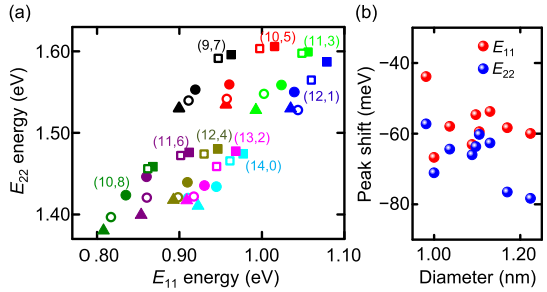

Figure 3. (a) Deposition thickness dependence of the E_{11} and E_{22} resonance energies for various chiralities. The data are obtained by the same procedure as in Figure 2. The excitation energy integration windows are from 1.44 to 1.63 eV for (9,7), (10,5), (11,3), and (12,1) or from 1.35 to 1.50 eV for the others. If the E_{11} resonance band is split into two as for the 3 nm sample in Figure 2a, we have obtained a peak area weighted average of the emission energy by fitting the spectrum with two Lorentz functions. The integration window for the emission energy is from 0.77 to 1.09 eV for all chiralities. The filled squares, open squares, filled circles, open circles, and filled triangles correspond to the samples before deposition, 3 nm sample, 7 nm sample, 16 nm sample, and 26 nm sample, respectively. (b) Peak shifts of the E_{11} and E_{22} resonance energies for the 26 nm sample relative to those before the deposition are shown as a function of the diameter. The error bars are smaller than the symbols.

chiralities measured, consistent with the dielectric screening effects due to the adsorbed molecules. The molecule-induced shifts of the E_{11} and E_{22} resonances for the 26 nm sample are plotted as a function of nanotube diameter in Figure 3b. Although we expect that the shifts become gradually smaller as the diameter increases,[30,35,36] there is no clear dependence. The scatter of the data points is likely caused by large tube-to-tube deviations of adsorption amounts. Averaging the shifts of the E_{11} and E_{22} resonances for all chiralities, we obtain values of −58 and −67 meV, respectively. Comparable emission energy shifts have been observed for nanotubes under dielectric screening by solvents,[30,37] explaining why the shifts due to organic molecule adsorption in solutions are suppressed.

We evaluate the change in the exciton resonance energy by considering the reduction of the electronic many-body interactions due to molecular adsorption. The E_{11} exciton energy is determined by $E_{11} = E_{sp} + E_{se} - E_{eb}$, where E_{sp} is the single-particle band gap, E_{se} is the self-energy from repulsive electron interactions, and E_{eb} is the exciton binding energy from the attractive electron−hole interactions.[38,39] Because the

DOI: 10.1021/acs.jpcc.8b12496
J. Phys. Chem. C 2019, 123, 5776−5781

magnitude of the self-energy is larger than that of the exciton binding energy, the E_{11} exciton energy is higher than E_{sp} by the net many-body correlation energy $E_{se} - E_{eb}$. Assuming that these interactions scale by the same factor C_X, the shift of the E_{11} exciton energy ΔE_{11} relative to the air-molecule adsorbed state is given by $\Delta E_{11} = (E_{se} - E_{eb}) \times (C_X - 1)$. For air-molecule-adsorbed nanotubes with 1 nm diameter, E_{se} and E_{eb} have been estimated to be 910 and 660 meV, respectively.[29] From the average ΔE_{11} of −58 meV for the 26 nm sample, C_X is calculated to be 0.77, which corresponds to a reduction of the many-body interactions with the molecular adsorption by 23%. Furthermore, C_X values for the 3 nm sample, 7 nm sample, and 16 nm sample are estimated to be 0.94, 0.83, and 0.78, respectively, showing that the many-body interaction energies reduce monotonically with increasing the molecular amounts. The absolute value of the average ΔE_{22} for the 26 nm sample is slightly larger than that of the average ΔE_{11}, which is reasonable because the net many-body correlation energy for the E_{22} excitons is larger than that for the E_{11} excitons.[30,40]

***T* Emission.** We now turn our attention to the low energy T emission. Figure 4a is a PLE map for a (9,7) nanotube in the

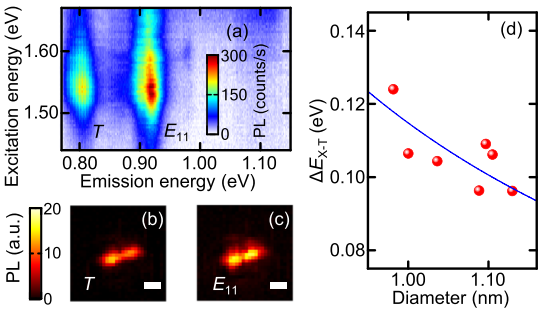

Figure 4. (a) PLE map for a (9,7) tube in the 26 nm sample. (b,c) PL images for T and E_{11} exciton emission, respectively, for the same tube. Spectral integration windows centered at 0.81 and 0.92 eV with a width of 10 meV are used for (b,c), respectively. Scale bars are 1 μm. (d) ΔE_{X-T} for the 26 nm sample is shown as a function of the diameter. All of the data are taken at P = 300 μW. The error bars are smaller than the symbols.

26 nm sample, and there are two peaks at 0.81 and 0.92 eV corresponding to the T and E_{11} emission, respectively. The absorption resonance energies for both emission are almost the same, and the PL images at the T and E_{11} energies overlap spatially (Figure 4b,c). The spectral and spatial coincidence indicates that the T emission comes from the same tube. We define the energy separation between the T and E_{11} peaks to be ΔE_{X-T}, for example ΔE_{X-T} = 0.11 eV in Figure 4a. The T emission energy for various chiralities is obtained by fitting the ensemble averaged PL spectra with a Lorentz function, and ΔE_{X-T} is plotted as a function of the diameter in Figure 4d. Because the K-momentum exciton emission should appear at 0.13−0.14 eV below the E_{11} emission peak,[32,34] it cannot explain the T emission with ΔE_{X-T} = 0.10−0.12 eV. In addition, intensity of the K-momentum exciton emission is typically 1% of the bright E_{11} exciton emission, but the T emission intensity can be comparable to the E_{11} emission.[34] A more plausible interpretation would be emission from trions, as the energy separation can be 0.10−0.14 eV under dielectric screening within the diameter range shown in Figure 4d.[41,42] The observed ΔE_{X-T} tends to become smaller as the diameter increases, consistent with the behavior for the exciton−trion energy separation.[28,34] As a trion is a bound state of a carrier and an exciton,[41] we expect trion formation if there is charge transfer between CuPc molecules and CNTs. Such a picture can also explain the E_{11} intensity reduction with the molecular adsorption. The weak dependence of the T emission intensity on deposition thickness is also consistent, as the first layer of CuPc should have formed for thickness larger than 7 nm.

The exciton−trion energy separation for the CuPc adsorbed state is smaller than that for the air molecule adsorbed state by about 70 meV for tubes with diameter d = 1 nm, indicating that exciton−carrier interactions are considerably screened by the CuPc molecules. It is known that the exciton−trion energy separation ΔE_{X-T} follows the relation $\Delta E_{X-T} = E_{tb} + E_{st}$, where $E_{tb} = A/d$ is the trion binding energy and $E_{st} = B/d^2$ is the singlet-triplet splitting energy while A and B are proportionality constants.[34,41] For the air molecule adsorbed state, A = 105 meV·nm and B = 70 meV·nm^2.[34] We fit the data by $\Delta E_{X-T} = (A/d + B/d^2) \times C_T$, under an assumption that both A and B scale by the same factor C_T upon the organic molecule adsorption. The result is shown as a blue line in Figure 4d, giving C_T = 0.67, which is comparable to the value of C_X.

Correlation between ΔE_{X-T} and E_{11}. So far we have been discussing the ensemble spectra, but data for the individual tubes provide additional insights to molecular screening effects on the many-body interactions. By fitting the PL spectra for each nanotube with the same procedure as the ensemble spectra, we obtain the energies for the T and E_{11} emission in various molecular screening environments. In Figure 5a, ΔE_{X-T} values for (9,7) individual nanotubes are plotted as a function of the E_{11} exciton emission energy. We find that there is a good correlation between ΔE_{X-T} and E_{11}, where ΔE_{X-T} becomes smaller as the E_{11} emission energy red shifts. We also plot data points for (9,7) suspended nanotubes with and

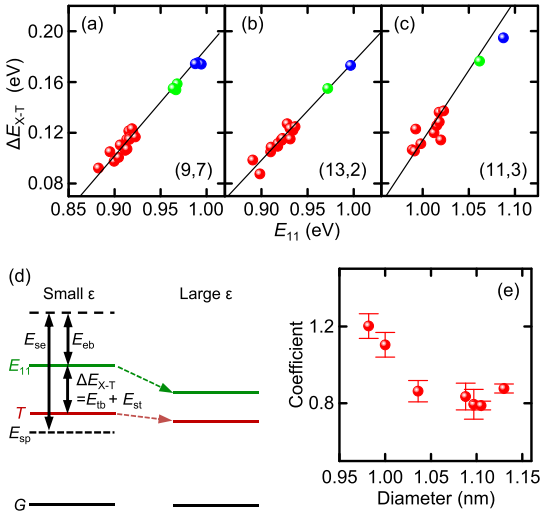

Figure 5. (a−c) Exciton−trion energy separation for (9,7), (13,2), and (11,3) tubes are shown as a function of the E_{11} emission energy. Red, green, and blue points are the results for CuPc adsorbed states, air-molecule adsorbed states, and pristine states without molecular adsorption, respectively. Note that the data points for the air-molecule adsorbed and pristine nanotubes are obtained from ref 28, where the trion emission for both states have been investigated by using field effect transistor structures. The error bars are smaller than the symbols. (d) Schematic diagram for tuning of the many-body interaction energies with the dielectric constant. (e) Coefficient for the correlation is shown as a function of the diameter.

DOI: 10.1021/acs.jpcc.8b12496
J. Phys. Chem. C 2019, 123, 5776−5781

without air-molecule adsorption from ref 28 as green and blue points, respectively. These data points also follow the trend, suggesting that there is a universal relation applicable to nanotubes under different surface conditions. Similar correlation is observed for (13,2) and (11,3) nanotubes (Figure 5b,c, respectively), as well as for the other chiralities. We note that CuPc adsorption can shift the E_{11} energy by ∼100 meV compared to the pristine state, offering flexible tunability over the emission energy.

The correlation can be understood in terms of the molecular dielectric screening (Figure 5d). In general, the many-body interactions determining the T and E_{11} exciton energies are sensitive to environment, which can simply be parameterized as the environmental dielectric constant ε. Assuming that interaction energies scale as $\varepsilon^{-\alpha}$ with α being a constant,[29,38] $\Delta E_{X-T} = E_{tb}^{\varepsilon=1}\varepsilon^{-\alpha} + E_{st}^{\varepsilon=1}\varepsilon^{-\alpha}$ and $E_{11} = E_{sp} + E_{se}^{\varepsilon=1}\varepsilon^{-\alpha} - E_{eb}^{\varepsilon=1}\varepsilon^{-\alpha}$, where $E_{tb}^{\varepsilon=1}$, $E_{st}^{\varepsilon=1}$, $E_{se}^{\varepsilon=1}$, and $E_{eb}^{\varepsilon=1}$ are the trion binding energy, singlet−triplet splitting energy, self-energy, and exciton binding energy at $\varepsilon = 1$, respectively. The slope for the correlation is then given by $\frac{\partial \Delta E_{X-T}}{\partial E_{11}} = \frac{E_{tb}^{\varepsilon=1} + E_{st}^{\varepsilon=1}}{E_{se}^{\varepsilon=1} - E_{eb}^{\varepsilon=1}}$, indicating a linear relation between ΔE_{X-T} and E_{11}. The experimentally observed correlation therefore implies that the many-body interaction energies scale similarly within the experimental conditions explored, which is reasonable because the scaling factor for the E_{11} exciton C_X is comparable to that for the trion C_T.

Using the reported values for pristine suspended nanotubes of $E_{tb}^{\varepsilon=1}$ = 117 meV, $E_{st}^{\varepsilon=1}$ = 78 meV, $E_{se}^{\varepsilon=1}$ = 980 meV, and $E_{eb}^{\varepsilon=1}$ = 725 meV for 1 nm diameter tubes,[28,29] the proportionality coefficient is about 0.8. To compare this value with the experimental results, we fit the data points for the organic molecule adsorbed state with a linear function. We impose the line to go through a data point for the air-molecule adsorbed state, where the E_{11} emission energy is obtained from the table in ref 25 and ΔE_{X-T} is determined from the equation given in ref 34. The obtained coefficients range from 0.8 to 1.2 (Figure 5e), which is a reasonable agreement considering the large uncertainty in the absolute value of $E_{se}^{\varepsilon=1}$.

CONCLUSIONS

In summary, we have investigated adsorption effects of CuPc molecules on excitons and trions in air-suspended CNTs by measuring PL spectra of the CuPc/CNT hybrids. By averaging the PLE spectra for tubes with the same chiralities, the red shift of the E_{11} and E_{22} resonances has been observed with increasing deposition thickness due to the molecular screening. The E_{11} energy modification from the pristine state to the CuPc adsorbed state can reach 100 meV, which is significantly larger than the energy shift with organic molecule adsorption in solutions. Furthermore, we find that the trion emission emerges at an energy lower than the E_{11} exciton emission, which is likely due to charge transfer between CuPc molecules and CNTs. The spectra from individual tubes show that there is a good correlation between the exciton−trion energy separation and the exciton emission energy. A model assuming power law scaling of the many-body interactions with dielectric constant can quantitatively explain the observed correlation, which should be able to describe nanotubes with different surface conditions in a universal manner. Our findings show that organic molecule adsorption significantly affects many-body interaction energies of suspended CNTs, which opens up a pathway to CNT devices utilizing noncovalent molecular functionalization.

AUTHOR INFORMATION

Corresponding Author

*E-mail: yuichiro.kato@riken.jp.

ORCID

Keigo Otsuka: 0000-0002-6694-0738

Yousoo Kim: 0000-0001-7730-0704

Yuichiro K. Kato: 0000-0002-9942-1459

Notes

The authors declare no competing financial interest.

ACKNOWLEDGMENTS

Work supported in part by RIKEN (Incentive Research Project), JSPS (KAKENHI JP16H05962 and JP17H07359), and MEXT (Nanotechnology Platform). We thank the Advanced Manufacturing Support Team at RIKEN for technical assistance.

REFERENCES

(1) Hirsch, A. Functionalization of single-walled carbon nanotubes. *Angew. Chem., Int. Ed.* **2002**, *41*, 1853−1859.

(2) Miyauchi, Y.; Iwamura, M.; Mouri, S.; Kawazoe, T.; Ohtsu, M.; Matsuda, K. Brightening of excitons in carbon nanotubes on dimensionality modification. *Nat. Photonics* **2013**, *7*, 715−719.

(3) He, X.; Hartmann, N. F.; Ma, X.; Kim, Y.; Ihly, R.; Blackburn, J. L.; Gao, W.; Kono, J.; Yomogida, Y.; Hirano, A.; et al. Tunable room-temperature single-photon emission at telecom wavelengths from sp3 defects in carbon nanotubes. *Nat. Photonics* **2017**, *11*, 577−582.

(4) Guldi, D. M.; Rahman, G. M. A.; Zerbetto, F.; Prato, M. Carbon nanotubes in electron donor-acceptor nanocomposites. *Acc. Chem. Res.* **2005**, *38*, 871−878.

(5) Ehli, C.; Oelsner, C.; Guldi, D. M.; Mateo-Alonso, A.; Prato, M.; Schmidt, C.; Backes, C.; Hauke, F.; Hirsch, A. Manipulating single-wall carbon nanotubes by chemical doping and charge transfer with perylene dyes. *Nat. Chem.* **2009**, *1*, 243−249.

(6) Malic, E.; Weber, C.; Richter, M.; Atalla, V.; Klamroth, T.; Saalfrank, P.; Reich, S.; Knorr, A. Microscopic model of the optical absorption of carbon nanotubes functionalized with molecular spiropyran photoswitches. *Phys. Rev. Lett.* **2011**, *106*, 097401.

(7) Bartelmess, J.; Ballesteros, B.; de la Torre, G.; Kiessling, D.; Campidelli, S.; Prato, M.; Torres, T.; Guldi, D. M. Phthalocyanine-pyrene conjugates: A powerful approach toward carbon nanotube solar cells. *J. Am. Chem. Soc.* **2010**, *132*, 16202−16211.

(8) Hecht, D. S.; Ramirez, R. J. A.; Briman, M.; Artukovic, E.; Chichak, K. S.; Stoddart, J. F.; Grüner, G. Bioinspired detection of light using a porphyrin-sensitized single-wall nanotube field effect transistor. *Nano Lett.* **2006**, *6*, 2031−2036.

(9) Alam, A.; Dehm, S.; Hennrich, F.; Zakharko, Y.; Graf, A.; Pfohl, M.; Hossain, I. M.; Kappes, M. M.; Zaumseil, J.; Krupke, R.; et al. Photocurrent spectroscopy of dye-sensitized carbon nanotubes. *Nanoscale* **2017**, *9*, 11205−11213.

(10) Joshi, A.; Ramachandran, C. N. Optoelectronic properties of cycloparaphenylene-carbon nanotube based molecular architectures. *J. Phys. Chem. C* **2018**, *122*, 19904−19912.

(11) Roquelet, C.; Garrot, D.; Lauret, J. S.; Voisin, C.; Alain-Rizzo, V.; Roussignol, P.; Delaire, J. A.; Deleporte, E. Quantum efficiency of energy transfer in noncovalent carbon nanotube/porphyrin compounds. *Appl. Phys. Lett.* **2010**, *97*, 141918.

(12) Correa, J. D.; Orellana, W. Optical response of carbon nanotubes functionalized with (free-base, Zn) porphyrins, and phthalocyanines: A DFT study. *Phys. Rev. B: Condens. Matter Mater. Phys.* **2012**, *86*, 125417.

(13) Orellana, W. Strong π-π interaction of porphyrins on (6,5) carbon nanotubes with full surface coverage: Ab-initio calculations. *Appl. Phys. Lett.* **2014**, *105*, 023110.

(14) Garrot, D.; Langlois, B.; Roquelet, C.; Michel, T.; Roussignol, P.; Delalande, C.; Deleporte, E.; Lauret, J.-S.; Voisin, C. Time-

DOI: 10.1021/acs.jpcc.8b12496
J. Phys. Chem. C 2019, 123, 5776−5781

resolved investigation of excitation energy transfer in carbon nanotube-porphyrin compounds. *J. Phys. Chem. C* **2011**, *115*, 23283−23292.
(15) Harvey, J. D.; Zerze, G. H.; Tully, K. M.; Mittal, J.; Heller, D. A. Electrostatic screening modulates analyte binding and emission of carbon nanotubes. *J. Phys. Chem. C* **2018**, *122*, 10592−10599.
(16) Zhao, J.-X.; Ding, Y.-H. Functionalization of single-walled carbon nanotubes with metalloporphyrin complexes: A theoretical study. *J. Phys. Chem. C* **2008**, *112*, 11130−11134.
(17) Casey, J. P.; Bachilo, S. M.; Weisman, R. B. Efficient photosensitized energy transfer and near-IR fluorescence from porphyrin-SWNT complexes. *J. Mater. Chem.* **2008**, *18*, 1510−1516.
(18) Zhong, Q.; Diev, V. V.; Roberts, S. T.; Antunez, P. D.; Brutchey, R. L.; Bradforth, S. E.; Thompson, M. E. Fused porphyrin-single-walled carbon nanotube hybrids: Efficient formation and photophysical characterization. *ACS Nano* **2013**, *7*, 3466−3475.
(19) Sarkar, R.; Habib, M.; Pal, S.; Prezhdo, O. V. Ultrafast, asymmetric charge transfer and slow charge recombination in porphyrin/CNT composites demonstrated by time-domain atomistic simulation. *Nanoscale* **2018**, *10*, 12683−12694.
(20) Stranks, S. D.; Sprafke, J. K.; Anderson, H. L.; Nicholas, R. J. Electronic and mechanical modification of single-walled carbon nanotubes by binding to porphyrin oligomers. *ACS Nano* **2011**, *5*, 2307−2315.
(21) Zhang, H.; Bork, M. A.; Riedy, K. J.; McMillin, D. R.; Choi, J. H. Understanding photophysical interactions of semiconducting carbon nanotubes with porphyrin chromophores. *J. Phys. Chem. C* **2014**, *118*, 11612−11619.
(22) Jašinskas, V.; Oberndorfer, F.; Paktas, V.; Hertel, T.; Gulbinas, V. Direct tracking of ultrafast carrier motion dynamics in semiconducting single-wall carbon nanotubes. *J. Phys. Chem. C* **2018**, *122*, 16424−16430.
(23) Lozzi, L.; Santucci, S.; Bussolotti, F.; La Rosa, S. Investigation on copper phthalocyanine/multiwalled carbon nanotube interface. *J. Appl. Phys.* **2008**, *104*, 033701.
(24) Basiuk, V. A.; Flores-Sánchez, L. J.; Meza-Laguna, V.; Flores-Flores, J. O.; Bucio-Galindo, L.; Puente-Lee, I.; Basiuk, E. V. Noncovalent functionalization of pristine CVD single-walled carbon nanotubes with 3d metal(II) phthalocyanines by adsorption from the gas phase. *Appl. Surf. Sci.* **2018**, *436*, 1123−1133.
(25) Ishii, A.; Yoshida, M.; Kato, Y. K. Exciton diffusion, end quenching, and exciton-exciton annihilation in individual air-suspended carbon nanotubes. *Phys. Rev. B: Condens. Matter Mater. Phys.* **2015**, *91*, 125427.
(26) Jiang, M.; Kumamoto, Y.; Ishii, A.; Yoshida, M.; Shimada, T.; Kato, Y. K. Gate-controlled generation of optical pulse trains using individual carbon nanotubes. *Nat. Commun.* **2015**, *6*, 6335.
(27) Tang, C. W. Two-layer organic photovoltaic cell. *Appl. Phys. Lett.* **1986**, *48*, 183−185.
(28) Uda, T.; Tanaka, S.; Kato, Y. K. Molecular screening effects on exciton-carrier interactions in suspended carbon nanotubes. *Appl. Phys. Lett.* **2018**, *113*, 121105.
(29) Lefebvre, J.; Finnie, P. Excited excitonic states in single-walled carbon nanotubes. *Nano Lett.* **2008**, *8*, 1890.
(30) Larsen, B. A.; Deria, P.; Holt, J. M.; Stanton, I. N.; Heben, M. J.; Therien, M. J.; Blackburn, J. L. Effect of solvent polarity and electrophilicity on quantum yields and solvatochromic shifts of single-walled carbon nanotube photoluminescence. *J. Am. Chem. Soc.* **2012**, *134*, 12485−12491.
(31) Caplins, B. W.; Mullenbach, T. K.; Holmes, R. J.; Blank, D. A. Femtosecond to nanosecond excited state dynamics of vapor deposited copper phthalocyanine thin films. *Phys. Chem. Chem. Phys.* **2016**, *18*, 11454−11459.
(32) Matsunaga, R.; Matsuda, K.; Kanemitsu, Y. Origin of low-energy photoluminescence peaks in single carbon nanotubes: *K*-momentum dark excitons and triplet dark excitons. *Phys. Rev. B: Condens. Matter Mater. Phys.* **2010**, *81*, 033401.
(33) Yasukochi, S.; Murai, T.; Moritsubo, S.; Shimada, T.; Chiashi, S.; Maruyama, S.; Kato, Y. K. Gate-induced blueshift and quenching of photoluminescence in suspended single-walled carbon nanotubes. *Phys. Rev. B: Condens. Matter Mater. Phys.* **2011**, *84*, 121409.
(34) Yoshida, M.; Popert, A.; Kato, Y. K. Gate-voltage induced trions in suspended carbon nanotubes. *Phys. Rev. B: Condens. Matter Mater. Phys.* **2016**, *93*, 041402.
(35) Schuettfort, T.; Nish, A.; Nicholas, R. J. Observation of a type II heterojunction in a highly ordered polymer-carbon nanotube nanohybrid structure. *Nano Lett.* **2009**, *9*, 3871−3876.
(36) Choi, J. H.; Strano, M. S. Solvatochromism in single-walled carbon nanotubes. *Appl. Phys. Lett.* **2007**, *90*, 223114.
(37) Ohno, Y.; Iwasaki, S.; Murakami, Y.; Kishimoto, S.; Maruyama, S.; Mizutani, T. Excitonic transition energies in single-walled carbon nanotubes: Dependence on environmental dielectric constant. *Phys. Status Solidi B* **2007**, *244*, 4002−4005.
(38) Walsh, A. G.; Vamivakas, A. N.; Yin, Y.; Cronin, S. B.; Ünlü, M. S.; Goldberg, B. B.; Swan, A. K. Screening of excitons in single, suspended carbon nanotubes. *Nano Lett.* **2007**, *7*, 1485−1488.
(39) Miyauchi, Y.; Zhang, Z.; Takekoshi, M.; Tomio, Y.; Suzuura, H.; Perebeinos, V.; Deshpande, V. V.; Lu, C.; Berciaud, S.; Kim, P.; et al. Tunable electronic correlation effects in nanotube-light interactions. *Phys. Rev. B: Condens. Matter Mater. Phys.* **2015**, *92*, 205407.
(40) Sato, K.; Saito, R.; Jiang, J.; Dresselhaus, G.; Dresselhaus, M. S. Discontinuity in the family pattern of single-wall carbon nanotubes. *Phys. Rev. B: Condens. Matter Mater. Phys.* **2007**, *76*, 195446.
(41) Matsunaga, R.; Matsuda, K.; Kanemitsu, Y. Observation of charged excitons in hole-doped carbon nanotubes using photoluminescence and absorption spectroscopy. *Phys. Rev. Lett.* **2011**, *106*, 037404.
(42) Santos, S. M.; Yuma, B.; Berciaud, S.; Shaver, J.; Gallart, M.; Gilliot, P.; Cognet, L.; Lounis, B. All-optical trion generation in single-walled carbon nanotubes. *Phys. Rev. Lett.* **2011**, *107*, 187401.

DOI: 10.1021/acs.jpcc.8b12496
J. Phys. Chem. C 2019, 123, 5776−5781